

# Multi-dimensional design and thermal protection capability of a regenerative cooled RBCC variable-geometry combustor

Liang Zhang<sup>1</sup>, Tingting Jing<sup>1\*</sup>, Xing Sun<sup>1</sup>, Tian Gao<sup>1</sup>, Zhen Xu<sup>1</sup>, Fei Qin<sup>1</sup>

1. National Key Laboratory of Solid Rocket Propulsion, Northwestern Polytechnical University, 710072, Xi'an, China

#### **Abstract**

The Rocket-based Combined-Cycle (RBCC) engine is a propulsion system that combines a ramjet engine with a rocket engine, which is capable of operating over a wide speed and space range. To ensure efficient operation throughout the flight envelope, variable geometry combustor is commonly used in RBCC engines to obtain higher performance under different operating conditions. However, non-uniform heat release during multimode operations should be considered with special attention and it is necessary to conduct research on the thermal protection system design of variable geometry combustor. This research proposes a multidimensional fast design method for regenerative cooling structure. The effectiveness of this regenerative cooling structure is simulated under different cooling equivalent ratios. The results indicate that the thermal environment is highly inhomogeneous. Results from one-dimensional design model indicate that the cooling effect of the structure is optimal when the cooling channel width is 2mm, the rib width is 3mm, and the height is 1mm. The cooling effect becomes progressively better as the cooling equivalent ratio increases. Three dimensional numerical calculations considering combustion, flow, supercritical-pressure heat transfer and fuel pyrolysis were further performed to analyze the thermal protection capability of the regenerative cooling structure at cooling equivalent ratios of 1.0, 1.5. The study indicates that when the cooling equivalent ratio is 1.0, the combustor experiences local over-temperature phenomenon, which appears at the side and bottom of the combustor. However, when the ratio is 1.5, the combustor operates normally with a maximum wall temperature of 1480 K, which is below the permissible temperature of 1500 K (assuming a Zirconia coating). Additionally, the fuel is completely cracked and the fuel heat sink is fully utilized. The results obtained here will lay the foundation for the future development of regenerative cooled RBCC engine with variable structure.

**Keywords:** RBCC, regenerative cooling, thermal protection system, variable-geometry combustor, convection heat transfer

#### 1. Introduction

Rocket-Based Combined Cycle (RBCC) engine is a propulsion system in the field of aerospace that combines a ramjet engine with a rocket engine, enabling a wide operational range. The future near-space hypersonic platforms and transatmospheric maneuvering vehicles pose higher requirements on the engine's length and thrust adjustment capabilities. Therefore, the adoption of a variable-geometry combustor allows the RBCC engine to adapt to the variations in different freestream parameters and combustor operating conditions. This approach enables the RBCC engine to achieve higher flexibility and adjustable comprehensive performance in complex multi-mode operating conditions [1]. The French WRR ramjet engine is a dual-fuel wide-range ramjet engine that utilizes hydrocarbon fuel and hydrogen fuel. It incorporates a variable-geometry intake duct and combustor technology to enhance its operational range. The combustor features a fixed 8° expansion surface on the lower wall and a five-segment hinged structure with movable plates on the upper wall. Three hydraulic actuators control three of the segments, while the remaining two segments are self-adaptive for adjustment. All operating mechanisms and hinges are located within a high-pressure chamber to prevent the impact of high-temperature gases on the

operating mechanisms [2-4]. Jicheng Ma proposed a transient one-dimensional model for the supercharged ramjet engine, which includes a flow combustion module and a regenerative cooling module. Through steady-state characteristic analysis of this model, it was discovered that, under the same flight Mach number and equivalent ratio, the maximum fuel equivalent ratio allowed in a regenerative-cooled supercharged ramjet engine is lower than that in an uncooled supercharged ramjet engine, while the thrust is higher in the regenerative-cooled engine compared to the uncooled supercharged ramjet engine. Moreover, for different control objectives such as thrust, stability, and kerosene temperature at the outlet of the cooling channels, responsive proportional-integral controllers were designed. Different control strategies were created for the two-stage kerosene injection regulation, ensuring the engine rapidly recovers to a safe state during mode transitions and wall surface overheating[5,6]. Jing Tingting from Northwestern Polytechnical University analyzed the thermal environment of a variable-geometry throat combustor under Ma6 engine operating conditions. The study involved zero-dimensional analysis for cold and hot source matching and onedimensional analysis for the design of parallel cooling channel structures. Furthermore, the effectiveness of the thermal protection scheme was verified through flow-heat asynchronous coupled numerical calculations[7].

Based on the current research foundation, this study proposes a multidimensional rapid design method for regenerative cooling structures. Using this method, the regenerative cooling structure of the variable-geometry combustor is designed considering different freestream conditions. Numerical simulations are conducted, at Ma6, with varying cooling equivalent ratios and the effectiveness of the regenerative cooling structure is analyzed.

#### 2. Method

### 2.1 Physical model description

This study focuses on the investigation of a specific variable-geometry RBCC (Rocket-Based Combined Cycle) engine. The RBCC engine operates in a wide speed range. The overall schematic diagram of the engine's configuration, including the inlet duct, isolation section, variable-geometry combustor, and exhaust nozzle (Figure 1). The operating mechanism is located at the rear of the combustor, and it adjusts the geometric throat area of the engine through rotational motion. Combined with the hydrocarbon fuel injection strategy, it enables the realization of different combustor configurations required for various flight Mach numbers. During the engine operation, the throat height is dynamically adjusted based on the incoming Mach number, allowing the hydrocarbon fuel to undergo combustion and release heat ahead of the geometric throat region.

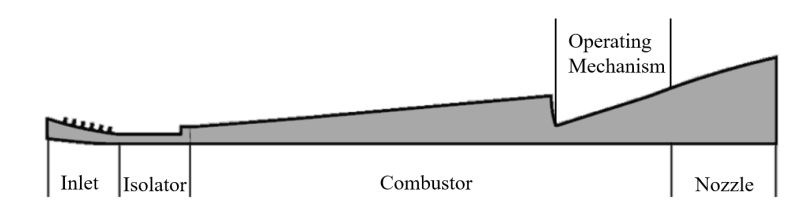


Figure 1. Schematic diagram of the variable-geometry RBCC engine configuration

#### 2.2 Numerical method

# 2.2.1 Governing equations

This study employs the following conservation equations for mass, momentum, energy, and species:

$$\frac{\partial(\bar{\rho}\tilde{u}_i)}{\partial x_i} = 0 \tag{1}$$

$$\frac{\partial(\bar{\rho}\tilde{u}_i)}{\partial x_i} = 0$$

$$\frac{\partial(\bar{\rho}\tilde{u}_i\tilde{u}_j)}{\partial x_j} = \bar{\rho}g_i - \frac{\partial\bar{p}}{\partial x_i} + \frac{\partial\tilde{\tau}_{\text{dee}}}{\partial x_j}$$
(2)

$$\frac{\partial \left(\bar{\rho}\tilde{u}_{j}\tilde{e}_{t}^{*}\right)}{\partial x_{i}} = \frac{\partial}{\partial x_{i}} \left(\lambda_{\text{dee}} \frac{\partial \tilde{T}}{\partial x_{i}}\right) - \frac{\partial \left(\bar{p}\tilde{u}_{j}\right)}{\partial x_{i}} \tag{3}$$

$$\frac{\partial \left(\bar{\rho}\tilde{u}_{j}\tilde{Y}_{k}\right)}{\partial x_{j}} = -\frac{\partial}{\partial x_{j}}\left(\bar{\rho}\tilde{u}_{d,k}\tilde{Y}_{k}\right) + \tilde{S}_{k} \tag{4}$$

In the equation,  $\rho$  represents the density of the fluid, u represents the velocity of the fluid,  $g_i$ represents the gravitational vector,  $e_t$  represents the total energy of the fluid, and T represents the temperature of the fluid. In the momentum equation,  $\tilde{\tau}_{de}$  represents the viscous stress term of the fluid, and its expression is given by equation (5).

$$\tilde{\tau}_{\text{dee}} = 2\mu_{eff} \left( \tilde{S}_{ij} - \frac{1}{3} \frac{\partial \tilde{u}_l}{\partial x_l} \delta_{ij} \right) \tag{4}$$

In the given equation,  $\mu_{de}$  represents the sum of dynamic viscosity and turbulent viscosity ( $\mu_{de}$ =  $\mu_s + \mu$ ) .  $\tilde{S}_{ij}$  represents the strain rate tensor, as shown in equation (6).

$$\tilde{S}_{ij} = \frac{1}{2} \left( \frac{\partial \tilde{u}_i}{\partial x_i} + \frac{\partial \tilde{u}_j}{\partial x_i} \right) \tag{5}$$

In the energy equation's diffusion term,  $\lambda_{de}$  represents the effective thermal conductivity coefficient after accounting for turbulent diffusion, and its expression is given by equation (7).

$$\lambda_{\text{dee}} = \lambda + \frac{\mu_t c_p}{P r_t} \tag{7}$$

When considering the cracking reaction of the coolant, the chemical reaction source term  $\tilde{S}_k$  in the species transport equation is given by equation (8).

$$\tilde{S}_k = M_{wk} \dot{\omega}_k \tag{8}$$

 $\tilde{S}_k = M_{wk} \dot{\omega}_k \tag{8}$  In the equation,  $M_{wk}$  represents the molar mass of component k, and  $\dot{\omega}_k$  represents the net production rate of that component.

Turbulence modeling in the aerospace field employs the SST k-□model, where the turbulent kinetic energy equation and the turbulent dissipation rate equation are given by equations (9) and (10).

$$\frac{\partial(\rho k)}{\partial t} + \frac{\partial(\rho k u_i)}{\partial X_i} = \frac{\partial}{\partial X_j} \left( \Gamma_k \frac{\partial k}{\partial X_j} \right) + G_k - Y_k + S_k \tag{9}$$

$$\frac{\partial(\rho\omega)}{\partial t} + \frac{\partial(\rho\omega u_i)}{\partial x_i} = \frac{\partial}{\partial x_i} \left( \Gamma_\omega \frac{\partial\omega}{\partial x_j} \right) + G_\omega - Y_\omega + D_\omega + S_\omega \tag{10}$$

In the equation,  $G_k$  represents the turbulent kinetic energy,  $G_\omega$  represents the  $\omega$  equation,  $\Gamma_k$ represents the effective diffusion term of k ,  $\varGamma_{\omega}$  represents the effective diffusion term of  $\omega$  , represents the divergence term of k,  $Y_{\omega}$  represents the divergence term of  $\omega$ , and  $D_{\omega}$  represents the orthogonal divergence term.

Furthermore, the governing equation for the solid domain is the Fourier heat conduction equation, and its expression is given by equation (11).

$$q = -\lambda \frac{dT}{dx} \tag{11}$$

The governing equation for the fluid-structure coupled wall surface is given by equation (12).

$$-\lambda \left(\frac{\mathsf{c}T}{\mathsf{c}x}\right)_w = h(T_w - T_f) \tag{12}$$

# 2.2.2 Materials and properties

The solid material used in this study for the engine is GH3536. It can be used for a long time below 1173K and for a short time at 1353K, without considering the zirconia coating. The density of the material is 8.28g/cm<sup>3</sup>. For detailed information on the thermal properties of this material refer to the literature [13].

In this study, the typical hydrocarbon fuel HF-1 [8] is employed as the coolant in the aerospace domain. The simplified three-step quasi-global chemical kinetics model [9], consisting of 17 components, is utilized for numerical simulation and analysis.

Thermodynamic properties such as density and specific heat are calculated using the Peng-Robinson

two-parameter real gas equation of state. On the other hand, transport properties such as thermal conductivity and viscosity are determined using empirical formulas and the mass-weighted mixture law

Regarding the thermal physical properties of aviation kerosene, comprehensive validations have been conducted in previous publications [10-12].

## 3. Results and Discussions

# 3.1 Thermal environment analysis

In this study, a numerical simulation of combustion with the equivalent ratio of 1.0 was conducted on a semi-model of the engine depicted in Figure 1. The injection method employed was wall injection. Considering that GH3536's short-term working temperature can reach up to 1,353K, we have retained a part of the safety margin and taken into account the thermal insulation effect of the zirconia coating. So the wall temperature of the combustor was set at 1500K to obtain the surface heat flux.

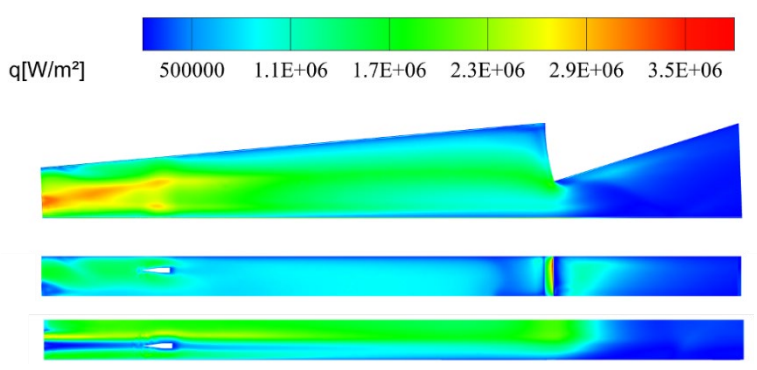


Figure 2. Surface heat flux

As shown in Figure 2, the thermal environment inside the variable-geometry combustor exhibits significant non-uniformity. The surface heat flux in the variable-geometry combustor ranges from a minimum of only 0.5 MW/m² to a maximum of up to 3.5 MW/m².

The side surface of the variable-geometry combustor exhibit higher surface heat flux compared to the upper and lower walls. Additionally, due to the proximity of HF-1 combustion near the side surfaces, irregular band-like regions with high heat flux are observed on the side surface. As the variable-geometry combustor expands, this phenomenon gradually improves. The surface heat flux in the band-like region decreases along the flow direction from approximately 3 MW/m² to around 1.7 MW/m². The region with the maximum surface heat flux is the geometric throat contraction surface (actuator mechanism wall) in the combustor. This is due to the approaching stagnation state of the main gas flow in this region, resulting in a high surface heat flux of up to 3.5 MW/m².

# 3.2 Cooling channel design and optimization

# 3.2.1Effect of cooling channel's size

Before conducting three-dimensional cooling structure design for the variable-geometry combustor, an optimization design of the cooling channels is performed using a one-dimensional code. Under the equivalent ratio of 1.0, a benchmark design point is set with a cooling channel width of 2mm and pin width of 3mm. By comparing the cooling effectiveness of different heights of cooling channels, the optimal cooling channel size with the best cooling performance is selected. The result is shown in Figure 3.

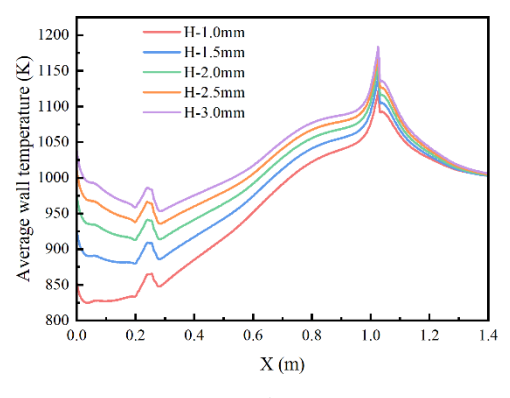


Figure 3. The along-channel average wall temperature with different heights

From Figure 3, it can be observed that cooling channels with different heights exhibit a consistent overall trend in the along-channel average wall temperature as obtained from the one-dimensional design calculations.

With the increase in channel height, although the flow area per channel increases, the flow rate of the coolant remains unchanged. This results in a reduction in the flow velocity of the coolant within the channel, leading to an increase in the maximum average wall temperature. As the channel height increases, the highest average wall temperature rises from 1092K to around 1135K, and the along-channel average wall temperature gradually increases.

Simultaneously, it can be observed that reducing the cooling channel width from 2mm to 1mm leads to a noticeable decrease in the along-channel average wall temperature due to the increased the velocity of coolant resulting from the reduced flow area. However, for channel heights of 2mm and above, the effect of increased the increased the velocity of coolant due to the reduced flow area on the along-channel average wall temperature reduction is limited. This indicates that within the range of cooling channel heights of 1-2mm, the increased the velocity of coolant is an important influencing factor for the along-channel wall temperature, i.e., the cooling effectiveness.

In addition to comparing the along-channel average wall temperature, the study also compared the outlet temperature, cracking rate, and pressure drop of the HF-1 for different channel heights. The results are shown in Table 1.

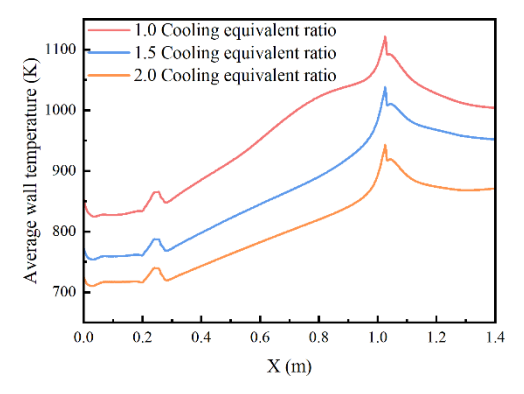
Table 1. The outlet temperature, cracking rate, and pressure drop of HF-1 under different channel height conditions

_					
	Channel height/mm	Outlet temperature/K	Cracking rate/%	Pressure drop/kPa	
	1.0	911.35	59.26	355.22	
	1.5	897.27	59.37	123.15	
	2.0	887.69	59.12	60.63	
	2.5	880.41	58.85	35.74	
	3.0	874.56	58.60	23.48	

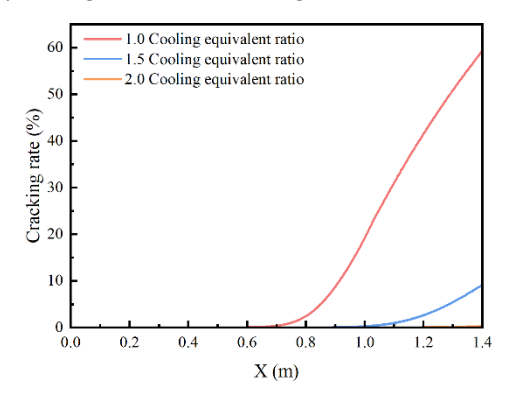
Based on the results, it can be observed that as the channel height increases from 1mm to 3mm, the outlet temperature of HF-1 decreases from 911.35K to 874.56K, and the cracking rate decreases from 59.26% to 58.60%. This indicates that as the channel height increases, the flow rate results in a decrease in the velocity of HF-1 within the channel. This process leads to a reduction in the surface convective heat transfer coefficient and weakens the convective heat transfer effect between HF-1 and the wall surface. Ultimately, this results in a weakened cooling effect, as illustrated in Figure 3. Meanwhile, according to the results, the corresponding pressure drop decreases with the increase of the channel height, and the pressure drop corresponding to the channel height of 1mm is 355.22kPa, which is still within the acceptable range considering the cooling effect, kerosene cracking and other factors.

# 3.2.2Effect of cooling equivalent ratio

After conducting the optimization design of channel dimensions, a comparison was made between the along-channel average wall temperature and the along-channel cracking rate of HF-1 under different cooling equivalent ratios. The results are shown in Figure 4.



#### (a) Along-channel average wall temperature



(c) Along-channel cracking rate of HF-1

Figure 4. The one-dimensional results of the along-channel average wall temperature and the cracking rate of HF-1

The results indicate that as the cooling equivalent ratio increases from 1.0 to 2.0, the maximum alongchannel average wall temperature decreases from 1305K to 1131K. Additionally, with the increase in cooling equivalent ratio, there is a noticeable overall decrease in the along-channel average wall temperature. It is worth noting that under cooling equivalent ratios of 1.5 and 2.0, the along-channel average wall temperature gradually increases from 0.6m to 0.9m. However, under the cooling equivalent ratio of 1.0, the upward trend of the average wall temperature in this segment is attenuated. within this section. By comparing the cracking rate of HF-1 along the flow path, it can be observed that under the cooling equivalent ratio of 1.0, cracking of HF-1 initiates at 0.6m along the flow path. In this section, the endothermic cracking reaction is the primary factor, leading to the absence of a significant temperature rise trend. Based on Figure 4, it can be observed that under the cooling equivalent ratio of 1.5, HF-1 undergoes slight cracking reactions at the rear of the combustor, with a final cracking rate of approximately 10%. However, under the cooling equivalent ratio of 2.0, HF-1 experiences minimal cracking, and only the physical heat sink of HF-1 is utilized without significant utilization of the chemical heat sink. This indicates that under the cooling equivalent ratio of 2.0, the utilization of HF-1 as a heat sink is low, resulting in overall lower cooling efficiency and wastage of the heat sink.

# 3.3 Thermal protection effectiveness simulation

After designing and optimizing the cooling channels of the variable-geometry combustor, based on the one-dimensional results, the final selection of cooling channel dimensions was determined as a channel width of 2mm, a height of 1mm, and a pin width of 3mm. These dimensions were used for the three-dimensional cooling structure design and establishment of the variable-geometry combustor. It should be noted that although the variable-geometry combustor was designed according to the Ma6 flow conditions, it also needs to consider low Mach number flow conditions. Therefore, a separate cooling structure is installed on the lateral side of the actuator mechanism to decouple the regenerative cooling structure from the actuator mechanism. This enables the regenerative cooling structure to operate effectively under different inflow Mach number conditions. The segmented regenerative cooling is shown in Figure 5.

#### Multi-Dimensional Design for RBCC Combustor Thermal Protection

Figure 5. Segmentation Diagram of the Regenerative Cooling Structure

After segmenting the overall three-dimensional regenerative cooling structure, considering the strong non-uniformity of the thermal environment in the variable-geometry combustor, multiple liquid collection chamber inlets are set at different segments of the three-dimensional cooling structure to avoid uneven flow distribution caused by this non-uniformity. Furthermore, the liquid coolant HF-1 is allocated with different flow rates based on this configuration: the coolant is cooled from the upper section, side section, and lower section, and then converged into the actuator mechanism for cooling. Finally, it enters the separate cooling structure for further cooling. This configuration is illustrated in Figure 5. After establishing the three-dimensional regenerative cooling structure, numerical simulations are conducted for cooling equivalent ratios of 1.0 and 1.5.

#### 3.3.1Cooling ratio = 1.0

The three-dimensional regenerative cooling structure was initially subjected to numerical simulations for the cooling equivalent ratio of 1.0. The heated wall temperature distribution of the regenerative cooling structure is shown in Figure 6.

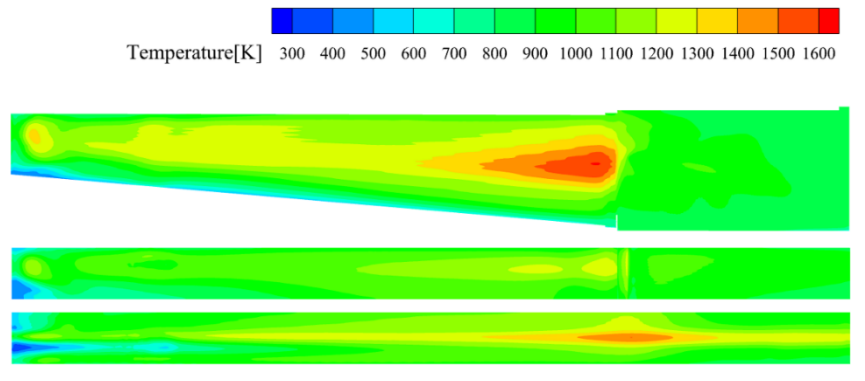


Figure 6. Wall temperature distribution of the regenerative cooling Structure under cooling equivalent ratio of 1.0

The results indicate that the upper section, side section, and lower section, where the coolant HF-1 has a lower flow rate, exhibit higher wall temperatures. Despite the actuator mechanism having the highest surface heat flux, the larger coolant flow rate results in lower wall temperatures after cooling. The highest temperature is approximately 1230K, and no localized overheating phenomenon is observed. The reason is that although the actuator mechanism exhibits the highest surface heat flux, the corresponding coolant HF-1 has a larger flow rate in this region. Each individual channel carries a higher flow rate with higher velocity. Consequently, the convective heat transfer coefficient on the channel surfaces is larger, resulting in enhanced cooling effectiveness.

The region with the highest wall temperature is located on the side section, reaching a maximum temperature of 1607K. Even considering the insulating effect of the zirconia coating, localized overheating still occurs in this area. The occurrence of this phenomenon can be attributed to two main factors. Firstly, due to the wall injection, the side section experience intense combustion reactions in the vicinity, leading to the irregular high heat flux regions mentioned earlier. Secondly, the side section has a larger heat dissipation area but a lower coolant flow rate, which contributes to the localized overheating phenomenon. Based on the aforementioned discussion, it is evident that the heat flux on the side wall surfaces exhibits significant non-uniformity. However, there is a notable improvement in the temperature distribution non-uniformity on the side wall surfaces. This indicates that modifying the inlet configuration of the liquid collection chambers based on the thermal environment can effectively address the flow distribution issues arising from thermal environment non-uniformity.

Not only did localized overheating occur on the side section, but also near the throat region on the

#### **Multi-Dimensional Design for RBCC Combustor Thermal Protection**

lower section, localized overheating phenomenon were observed with temperatures reaching approximately 1520K. The reason behind this is the higher heat flux on the corresponding wall surface, leading to increased flow resistance within the channel. As a result, the coolant flow in this region decreases, causing localized overheating to occur in the cooling channel.

In order to investigate the variation of HF-1 along the cooling channels of the regenerative cooling structure during its operation, the temperature and cracking rate of HF-1 were extracted from the upper section, side section, and lower section. The results are shown in Figure 7.

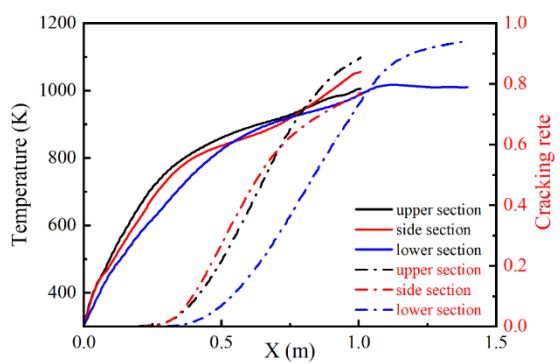


Figure 7. Along-channel temperature and cracking rate of three sections under cooling equivalent ratio of 1.0

The outlet temperature and cracking rate of HF-1 were recorded for the upper section, side section, and lower section. The statistical results are summarized in Table 2.

Table 2. Outlet temperature and cracking rate of three sections under cooling equivalent ratio of 1.0

	<u> </u>	<u> </u>
Location	Temperature(K)	Cracking rate(%)
upper section	1006.17	88.80
side section	1056.64	77.18
lower section	1010.30	94.15

The results indicate that the temperature and cracking rate of HF-1 exhibit three distinct stages of increase. In the initial stage, the temperature of HF-1 rapidly rises in all three sections, with no cracking reaction occurring. The upper section experiences the fastest temperature increase, followed by the side section, while the lower section exhibits the slowest temperature rise. During this stage, the sharp increase in HF-1 temperature can be attributed to the high heat flux at the front of all three sections. where the released heat from combustion is converted into physical heat sink for HF-1. In the second stage, the rate of temperature increase in HF-1 slows down, while the cracking rate starts to rapidly increase. HF-1 begins to undergo thermal crack, converting the absorbed heat from convective heat transfer into chemical energy. At this stage, the heat absorbed by HF-1 from convective heat transfer is primarily converted into chemical heat sink. During this stage, the dominant factor in the cooling process is the utilization of HF-1's chemical heat sink. It is worth noting that the behavior of HF-1 in the side section during the second stage differs from that of the upper and lower sections. In this stage, the temperature of HF-1 in the side section initially increases slowly, indicating the dominance of the chemical heat sink. However, it later rapidly rises, suggesting the combined effect of both the physical and chemical heat sinks. This phenomenon is confirmed by the outlet temperature and cracking rate measurements. The third stage is specific to the lower section, where the temperature of HF-1 ceases to increase and instead exhibits a slight decrease. This can be attributed to the intense cracking reaction occurring in HF-1 during this stage. The majority of the heat absorbed from convective heat transfer is utilized for the cracking reaction, converting it into chemical energy.

The above results indicate that under the cooling equivalent ratio of 1.0, this regenerative cooling structure exhibits localized overheating phenomenon, which can lead to structural failure. It is necessary to increase the cooling equivalent ratio to ensure the effectiveness of the structure.

# 3.3.2Cooling ratio = 1.5

After numerical simulations with the cooling equivalent ratio of 1.0, further simulations were performed with the cooling equivalent ratio of 1.5. The resulting heated wall temperature distribution of the regenerative cooling structure is shown in Figure 8.

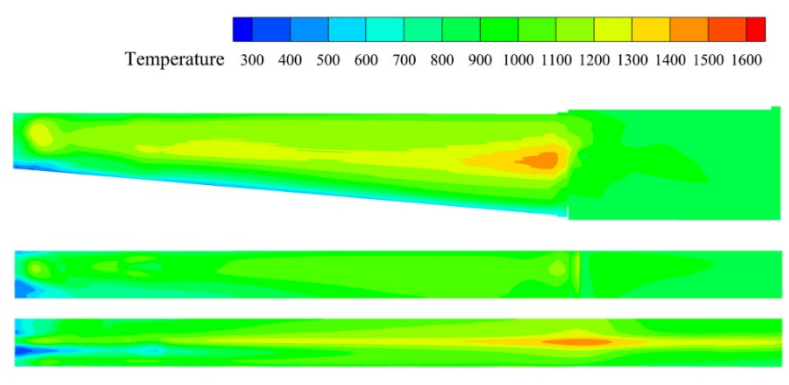


Figure 8. Wall temperature distribution of the regenerative cooling Structure under cooling equivalent ratio of 1.5

The results indicate that the overall trend of the wall temperature distribution is similar to that under the cooling equivalent ratio of 1.0. High-temperature regions are predominantly observed in the lower section and side section. However, the key difference is that the highest wall temperature is found in the lower section, reaching up to 1480K, while the highest temperature in the side section reaches 1450K. Considering the presence of zirconia coating, no overheating phenomenon was observed. Additionally, it can be observed that as the cooling equivalent ratio increases, the temperatures in the upper section, lower section, and side section all decrease significantly. The high-temperature region in the side section decreases in area, the temperature gradient in the high-temperature region decreases, and there is a noticeable reduction in the localized high-temperature region on the upper section.

In order to investigate the variation of HF-1 during the operation of the regenerative cooling structure, the temperature and cracking rate of HF-1 were extracted along the length of the upper section, side section, and lower section. The results are shown in Figure 9.

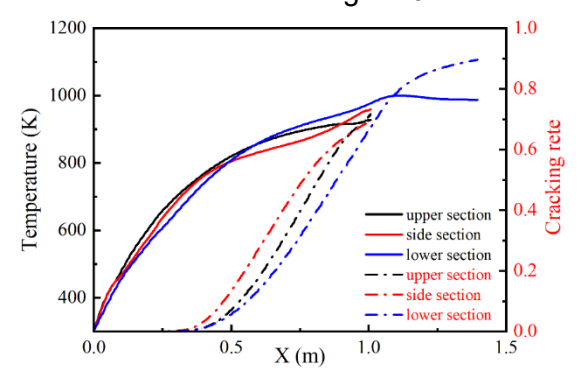


Figure 9. Along-channel temperature and cracking rate of three sections under cooling equivalent ratio of 1.5

The outlet temperature and cracking rate of HF-1 were recorded for the upper section, side section, and lower section. The statistical results are summarized in Table 3.

Table 3. Outlet temperature and cracking rate of three sections under cooling equivalent ratio of 1.5

Location	Temperature(K)	Cracking rate(%)
upper section	928.07	71.72
side section	960.03	69.99
lower section	987.55	89.63

The results indicate that compared to the numerical simulation results with the cooling equivalent ratio of 1.0, there is a varying degree of decrease in the outlet temperature and cracking rate of HF-1 in all three sections. Based on the line graphs of the along-channel temperature and cracking rate of HF-1 of the three sections, it can be observed that the variation process of HF-1 in all three sections can still be divided into three stages. In the first stage, HF-1 in all three sections does not undergo cracking, and the heat absorbed from convective heat transfer is converted into physical heat sink, leading to a rapid increase in HF-1 temperature. In the second stage, the cracking rate of HF-1 in all three sections increases rapidly, while the temperature rise slows down. This is because during this stage, a cracking reaction occurs, converting a portion of the heat absorbed from convective heat transfer into chemical

#### **Multi-Dimensional Design for RBCC Combustor Thermal Protection**

energy of the cracking products. It is worth noting that compared to the numerical simulation results with the cooling equivalent ratio of 1.0, the occurrence of the cracking reaction in HF-1 is delayed.

Under the cooling equivalent ratio of 1.5, the third stage is no longer exclusive to the lower section. In this stage, the upper section of HF-1 exhibits a decrease in temperature as the cracking rate increases. This indicates that in this stage, the heat absorbed by HF-1 in the upper and lower sections from convective heat transfer is primarily utilized for the occurrence of the cracking reaction, converting into chemical energy of the cracking products.

Based on the numerical simulation results, under the cooling equivalent ratio of 1.5, this regenerative cooling structure no longer exhibits localized overheating phenomenon. This validates the effectiveness of the regenerative cooling structure under the cooling equivalent ratio of 1.5. However, under the condition of the cooling equivalent ratio of 1.5, the outlet temperature and cracking rate of HF-1 are relatively high, indicating a certain risk of coking.

#### 4. Conclusions

This study analyzed the thermal environment in the variable-geometry combustor of the engine, and optimized the dimensions of the cooling channels using a one-dimensional program, and a three-dimensional regenerative cooling structure was established. The regenerative cooling structure was built based on one-dimensional calculations. The convection heat transfer characteristics and thermal protection effectiveness of this regenerative cooling structure were analyzed by three-dimensional numerical simulations under different equivalent ratios. The following conclusions were obtained:

- (1) Due to the wall jet injection strategy of HF-1, the variable-geometry combustor exhibits significant non-uniformity in the thermal environment. The surface heat flux ranges from a minimum of 0.5 MW/m² to a maximum of 3.5 MW/m². Three-dimensional numerical simulation results show that the cooled combustor wall temperature also exhibits inhomogeneity due to the inhomogeneous combustor thermal environment. This phenomenon was improved by redistributing the flow rate at the inlet of the liquid collection chamber.
- (2) A rapid design and optimization of the regenerative cooling structure were performed using a onedimensional program, along with an evaluation of the influence of different cooling channel dimensions on the cooling effectiveness. The results indicate that a cooling channel with a width of 2mm, height of 1mm, and pin width of 3mm exhibits the optimal cooling performance.
- (3) Based on zero-dimensional analysis results, the variable-geometry combustion chamber exhibits a fuel heat sink requirement of 3.97 MJ/kg under the equivalent ratio of 1.0, whereas under the equivalent ratio of 1.5, the fuel heat sink requirement reduces to 2.64 MJ/kg. Consequently, even with the consideration of the high-temperature insulation properties of the zirconia coating, the engine is unable to operate properly under the equivalent ratio of 1.0. This is primarily attributed to the small scale of the engine, resulting in a mismatch between the fuel and the total heat release on the wall surface. However, under the equivalent ratio of 1.5, the engine is able to operate normally, thereby validating the effectiveness of the regenerative cooling structure.

# **Copyright Statement**

The authors confirm that they, and/or their company or organization, hold copyright on all of the original material included in this paper. The authors also confirm that they have obtained permission, from the copyright holder of any third party material included in this paper, to publish it as part of their paper. The authors confirm that they give permission, or have obtained permission from the copyright holder of this paper, for the publication and distribution of this paper as part of the ICAS proceedings or as individual off-prints from the proceedings.

#### References

- [1] Zhang. M. "Study on thermal structure scheme of RBCC variable structure combustor," Northwestern Polytechnic University, 2023.
- [2] Falempin F, Salmon T, Avrashkov V. Fuel-cooled composite materials structures Status at aerospatiale matra. 36th AIAA/ASME/SAE/ASEE Joint Propulsion Conference and Exhibit Las Vegas. 2000.
- [3] Bouchez M, Falempin F, Levine V, et al. French-Russian Partnership on Hypersonic Wide-Range Ramjets. *Journal of Propulsion and Power*, Vol. 17, No. 6, pp 1177-1183, 2001.
- [4] Bouchez M, Levine V. French-Russian Cooperation in High-Speed Air Breathing Propulsion. *AIAA International Air and Space Symposium and Exposition: The Next 100 Years* Dayton, Ohio, 2003.
- [5] Ma J, Chang J, Huang Q P, et al. Multi-objective coordinated control of regeneratively-cooled scramjet engine with two-stage kerosene injection. *Aerospace Science and Technology*, Vol. 90, pp 59-69, 2019.
- [6] Ma J, Chang J, Zhang J, et al. Control-oriented unsteady one-dimensional model for a hydrocarbon regeneratively-cooled scramjet engine. *Aerospace Science and Technology*, Vol. 85, pp 158-170, 2019.
- [7] Jing. T. "Study on regenerative cooling flow and heat transfer characteristics of hydrocarbon fuel RBCC combustor," Northwestern Polytechnic University, 2018.
- [8] Jiang R, Liu G, Zhang X. Thermal Cracking of Hydrocarbon Aviation Fuels in Regenerative Cooling Microchannels. *Energy Fuels* Vol. 27, pp 2563-77, 2013.
- [9] Jing T, He G, Li W, Zhang D, Qin F, Li R. Flow and thermal analyses of supercritical hydrocarbon fuel in curved regenerative cooling channel around cavity in rocket based combined cycle engine. *Applied Thermal Engineering*, Vol. 145, pp 423-34, 2018.
- [10]Xu K, Ruan B, Meng H. Validation and analyses of RANS CFD models for turbulent heat transfer of hydrocarbon fuels at supercritical pressures. *International Journal of Thermal Sciences* Vol. 124, pp 212-26, 2018.
- [11]Xu K, Meng H. Analyses of surrogate models for calculating thermophysical properties of aviation kerosene RP-3 at supercritical pressures. *Sci China Technol Sci*, Vol. 58, pp 510-8, 2015.
- [12]Sun X, Meng H. Large eddy simulations and analyses of hydrocarbon fuel heat transfer in vertical upward flows at supercritical pressures. *International Journal of Heat and Mass Transfer*, Vol. 170, 2021.
- [13] Editorial board of China Aviation Materials Handbook. *China Aeronautical Materials Handbook*. 2nd edition, Standards Press of China, 2013.